DOI: 10.1111/mice.13105

RESEARCH ARTICLE

COMPUTER-AIDED CIVIL AND INFRASTRUCTURE ENGINEERING WILEY

Neural operator for structural simulation and bridge health monitoring

Chawit Kaewnuratchadasorn[1,2] | **Jiaji Wang**[2] | **Chul-Woo Kim**[1]

[1]Department of Civil and Earth Resources Engineering, Kyoto University, Kyoto, Japan

[2]Department of Civil Engineering, The University of Hong Kong, Pok Fu Lam, Hong Kong

Correspondence
Chul-Woo Kim, C1-183, KyotoDaigaku-Katsura, Nishikyoku, Kyoto 615-8540, Japan.
Email: kim.chulwoo.5u@kyoto-u.ac.jp

Funding information
JSPS (Japan Society for the Promotion of Science) Postdoctoral Fellowship, Grant/Award Number: P22062; JSPS (Japan Society for the Promotion of Science) bilateral joint research projects, Grant/Award Number: JPJSBP120217405; The University of Hong Kong Start-up Fund for New Staff; The University of Hong Kong Seed Fund for Basic Research for New Staff

Abstract

Infusing deep learning with structural engineering has received widespread attention for both forward problems (structural simulation) and inverse problems (structural health monitoring). Based on Fourier neural operator, this study proposes VINO (Vehicle–Bridge Interaction Neural Operator) to serve as a surrogate model of bridge structures. VINO learns mappings between structural response fields and damage fields. In this study, vehicle–bridge interaction (VBI)–finite element (FE) data set was established by running parametric FE simulations of the VBI system, considering a random distribution of the structural initial damage field. Subsequently, vehicle-bridge interaction (VB)–experimental (EXP) dataset was produced by conducting an experimental study under four damage scenarios. After VINO was pretrained by VBI-FE and fine-tuned by VBI-EXP from the bridge at the healthy state, the model achieved the following two improvements. First, forward VINO can predict structural responses from damage field inputs more accurately than the FE model. Second, inverse VINO can determine, localize, and quantify damages in all scenarios, validating the accuracy and efficiency of data-driven approaches.

1 | INTRODUCTION

Because of the combination of repeated external loads, environmental degradation, earthquakes, and other disasters, the structural performance may decrease. Structural health monitoring (SHM) has become an important discipline in civil engineering, which aims to identify anomalies and detect structural degradation to mitigate deterioration or even collapses of structures in both inland and offshore (Brownjohn, 2006; Pezeshki et al., 2023). In transportation systems, bridges widely experience increased usage due to loads of growing traffic, wind, temperature, earthquake, or other environmental effects. Therefore, bridge health monitoring (BHM) has gained growing attention for maintenance purposes (Kot et al., 2021; Rizzo & Enshaeian, 2021).

Visual inspection and vibration-based BHM are two research topics in evaluating the performance of existing bridge structures. Conventional visual inspections are typically based on human visual inspections, while the computer vision–based inspection of bridges has also been developed recently. The visual inspections focus on detecting concrete cracking, concrete crushing, steel corrosion, and steel fracture of visible components. Conventional visual inspections are labor intensive, time-consuming, traffic interfering, and high cost (Flah et al., 2022; Hou

Chawit Kaewnuratchadasorn and Jiaji Wang contributed equally to this work.

& Xia, 2021). In addition, the visual inspection results may be subjective to inspectors' judgments (An et al., 2019). The vibration-based BHM adopts a data acquisition system to obtain vibration signals (i.e., displacement, rotation angle, acceleration, and strain) of the bridge through various sensors, including displacement sensors, gyro sensors, accelerometers, and strain gauges. Vibration-based BHM can detect the damage in bridge structures including both visible and invisible components. The advancements in data acquisition software and hardware have driven vibration-based BHM to become a promising solution for investigators, project managers, and infrastructure operators at the industrial level (Gharehbaghi et al., 2021). In BHM, the damage detection may be classified into four levels: Level 1 determines the existence of damage on a bridge; Level 2 localizes the damage along the span of the bridge; Level 3 quantifies the damage severity either globally or locally; and Level 4 predicts the remaining operation lifespan of the bridge. Most of the research focuses on the first three identification levels (Gharehbaghi et al., 2021; Hou & Xia, 2021).

BHM algorithms may be divided into model-driven (i.e., physics-informed) algorithms and data-driven algorithms. The BHM algorithms may also be divided into time-domain algorithms and frequency-domain algorithms. The frequency-domain algorithms generally identify the changes in modal parameters (i.e., frequency and modal shape) induced by damages and predict the damage distribution based on modal parameters. A number of research works have reported successful identifications of modal parameters through model updating or signal processing. For instance, Kankanamge et al. (2020) implemented various wavelet transofrm algorithms in BHM to identify modal parameters and to achieve damage detection of various bridges. Other research (Abeykoon et al., 2018; Cao et al., 2017) analyzed the damping coefficient from acceleration responses and classified undamaged and damaged structures by the differences in the coefficient. Yuen and Huang (2018) proposed an improved Bayesian substructure identification approach to model boundary forces of substructures and constraints to increase the identifiability of the inverse problem in terms of probability and its uncertainty level. Furthermore, Yuen et al. (2019) proposed self-calibration and Bayesian framework to estimate system state and identify the anomalies of bridge sections in real time. Li et al. (2016) applied a method to obtain modal parameters using wavelet and Hilbert transforms and verified it on Lotte World Tower. The study suggested a promising feasibility in the implementation on large real-life structures. Chang and Kim (2016) identified frequencies and modal damping ratios of each mode using multivariate autoregressive (MAR) model and detected the damages by Mahalanobis distance of collected modal parameters. However, the frequency-domain algorithms may not fully utilize the measured data in the time domain. In addition, the modal parameters may be too sensitive to environmental effects and it may be hard to infer the damage distribution based on the identification results of modal parameters (An et al., 2019; Kot et al., 2021; Yang & Lin, 2005).

Recent years have seen the accelerated development of artificial intelligence (AI) and its application to technology, science, and engineering (Hassanpour et al., 2019; Martins et al., 2020). Adeli and Kim (2001) employed the neural dynamic model to update design variables, evaluate cost, and analyze a structure for optimizing the cost of composition beams of concrete, steel beam, and shear studs. Rafiei and Adeli (2017a) utilized machine learning classification and neural dynamic optimization model to define the threshold of an earthquake and its location for an early warning system. Rafiei et al. (2017) applied Restricted Boltzmann Machine with deep belief to predict a 28-day compressive strength of concrete aggregates. Inputs of the model are the amount of seven compositions, and the model was able to achieve 98% in accuracy. The machine learning and deep learning approaches also gained more attention in the structural monitoring and damage detection fields. Oh et al. (2017) developed the evolutionary radial basis function neural network (ERBFN) to learn the relationship between wind and strain of building columns and verified the approach by data from wind tunnel test. Based on the results, ERBFN was capable of estimating the strain of columns for wind speed and direction, which helps evaluate the safety of a structure. Wang et al. (2022) compared and suggested that DeepLabv3+ with the ResNet101 backbone showed the greatest performance among all five state-of-the-art architectures and three backbones on the Crackv1 data set in crack detection for bridge monitoring purposes. In vibration-based SHM, many works provided a justification between undamaged and damaged states of a bridge through frameworks that integrate machine learning and the critical index for damages (Dackermann et al., 2010; Entezami et al., 2022; Fernandez-Navamuel et al., 2022). Rafiei and Adeli (2017b) compared machine learning classifications in detecting damage levels from inputs of transformed denoised acceleration responses. Perez-Ramirez et al. (2019) proposed a framework using empirical mode decomposition (EMD) to filter responses, mutual information (MI) to determine an optimal neural network, and Bayesian regularization to train a model to predict damage from different earthquake levels on a scaled bridge. Goi and Kim (2017) applied principal component analysis (PCA) on a vector autoregressive (VAR) model to extract features for the proposed damage index based on the hypothesis test. Bao et al. (2019) converted time-series responses into images and applied deep

neural network (DNN) to classify seven anomaly patterns (normal, missing, minor, outlier, square, trend, and drift), achieving 87% accuracy on the test set. Luo et al. (2019) applied window frame on long-term time-series data and classified impulse responses by deep auto-encoder (DAE), then indicated deterioration process by bridge health index. Iannelli et al. (2022) simulated spacecraft structure and added damages to generate structural responses. Then, the Long Short-Term Memory (LSTM) network was utilized to predict the damage scenario at the numerical level. Avci et al. (2021) reviewed the work conducted in the domain, which mainly employed artificial, fuzzy, and convolution neural networks (ANN, FNN, and CNN) with feature extraction and data processing to detect and localize damages; although most of the reviewed work reached over 90% accuracy, all required training data from both healthy structure and damaged structure. In addition, machine learning algorithms may be divided into supervised learning and unsupervised learning. The unsupervised learning models are more convenient to apply but difficult to determine the sensitivities, limitations, and practicality. The supervised models currently encounter difficulty in developing well-established data sets with labels of damage and are mostly validated only based on numerical data sets instead of experimental data sets (Gomez-Cabrera & Escamilla-Ambrosio, 2022). The supervised learning models may need training data of damaged structures, which may be impractical for BHM application (Azimi et al., 2020; Gordan et al., 2022; Malekloo et al., 2021; Toh & Park, 2020).

In response to the aforementioned challenges in BHM, this paper proposes the Vehicle–Bridge Interaction Neural Operator (VINO) framework for data-driven SHM and structural simulation. VINO adopts the Fourier neural operator (FNO; Li et al., 2020) architecture and is trained on the vehicle–bridge interaction (VBI) data set for the damage detection problem. As a new benchmark of deep learning architecture in solving partial differential equations, FNO is an encoder-decoded–based model, which is able to learn function mapping (Kovachki et al., 2021; Li et al., 2020). Two VBI data sets are generated in this study, including the numerical VBI data set based on finite element (FE) analysis (VBI-FE) and the experimental VBI data set based on laboratory experiments (VBI-EXP) on a scaled bridge. The fine-tuning approach is used to achieve damage detection of the scaled bridge. The pretrained model from the VBI-FE data set was fine-tuned only by experimental data from a healthy bridge (in VBI-EXP data set) to predict the data on the bridge at the damaged state. Therefore, the contributions are as follows:

1. This study introduces the VINO, which is an end-to-end framework to detect damage directly from the structural response and predict structural response directly from damage distribution. The VINO can be more accurate and faster than the FE model in predicting structural responses.
2. This study achieves a real-time all-in-one damage determination, localization, and quantification model by mapping between the structural damage field and the structural response field. The inverse VINO model map from the structural damage field to the structural response field.
3. This study predicts damages on a bridge at damaged states with only experimental data of healthy bridges using the fine-tuning method on the pretrained model.

In this paper, Section 2 describes the methodologies of VBI, FNO, and transfer learning in the proposed framework VINO. Then, Section 3 reveals the numerical (VBI-FE) and experimental (VBI-EXP) data sets for training, testing, fine-tuning, and validating VINO models. The numerical results of forward and inverse VINO for structural simulation and SHM are discussed in Section 4, and the performances on experimental data are reported in Section 5. Lastly, Section 6 summarizes the contribution of work and provides suggested future work for more practical data-driven research in bridge and structural engineering.

2 | METHODOLOGIES

2.1 | Background of VBI

VBI means the interaction between a moving vehicle and a bridge. To simulate the VBI effect, models typically consist of three main input components: bridge, vehicle, and road profile, which influence the outputs differently. The outputs from the simulation are the responses of the bridge and vehicle (displacement, velocity, and acceleration) at distinct time steps (Clough & Penzien, 1993; Kim et al., 2005; Yang & Lin, 2005).

For the bridge, researchers apply different types of bridge models in an FE model for specific applications, including beam element models, shell element models, solid element models, and hybrid models. In this study, the Euler–Bernoulli beam with simple support is considered to generate the output for machine learning applications. The parameters of the input bridge include the span length, number of beam elements, bridge mass per unit length, damping coefficient, elastic modulus, and moment of inertia. For damage detection purposes, a damage field (the distribution of damage along bridge length) can be added to the parameters to obtain a simulation of the damaged bridge.

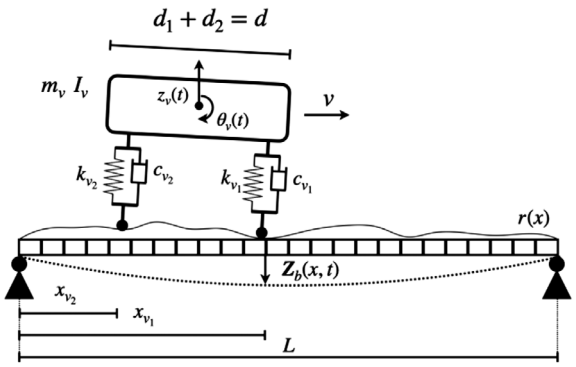

FIGURE 1 Vehicle–bridge interaction system consisting of a half-car model, element-segmented bridge, and road profile.

Various complexities of vehicle models have been seen in past studies. Vehicle models range from a simple single-vehicle force, which refers to a constant force moving on a bridge, to more complicated car models. Options in car models include quarter-car, half-car, and full-car, with different degrees of freedom. Therefore, the required parameters in the vehicle model include mass, the moment of inertia, the damping constant, the stiffness constant, the distance between axles, and vehicle speeds. Indeed, each component has a particular effect on bridge and vehicle responses in the simulation.

The road profiles (often referred to as road surface roughness) affect the dynamic responses of bridges and vehicles. ISO 8680 classified road profiles into eight classes from A to H (best to poorest). The profile is derived as a representative function of road surface roughness $r(x)$ as written in Equation (1) (ISO 8608, 2016).

$$r\ (x) = \sum_i d_i \cos\left(n_i x + \theta_i\right) \tag{1}$$

where x is the position along the bridge span; n_i denotes the ith spatial frequency; d_i and θ_i represent the roughness amplitude and phase angle, respectively. The roughness amplitude is determined for each class.

Figure 1 demonstrates the interaction of vehicle and bridge. The governing equations for the two-degree-of-freedom half-car model are shown in Equation (2) and Equation (3) to describe the system. In Figure 1, m_v and l_v stand for mass and moment of inertia of the vehicle; d_1 and d_2 are the space distance between the center of mass to the first and second axle, orderly; and k_{v_1} and k_{v_2} symbolize the spring constant of the axles; c_{v_1} and c_{v_2} denote the damping constant of the axles; x_{v_1} and x_{v_2} are the locations of the axles on the bridge; $z_v(t)$ represents the displacement of the vehicle in z-axis direction; $r(x)$ specifies roughness at position x; and L designates bridge span length.

$$\begin{aligned} 0 = {} & m_v\, \ddot{z}\,(t) \\ & + c_{v_1}\left[\dot{z}_v\,(t) + d_1\dot{\theta}_v\,(t) - \left\{\mathbf{I}_b\left(x_{v_1}\right)\right\}^T\left\{\dot{\mathbf{Z}}_b\,(t) + v r'\left(x_{v_1}\right)\right\}\right] \\ & + c_{v_2}\left[\dot{z}_v\,(t) + d_2\dot{\theta}_v\,(t) - \left\{\mathbf{I}_b\left(x_{v_2}\right)\right\}^T\left\{\dot{\mathbf{Z}}_b\,(t) + v r'\left(x_{v_2}\right)\right\}\right] \\ & + k_{v_1}\left[z_v\,(t) + d_1\theta_v\,(t) - \left\{\mathbf{I}_b\left(x_{v_1}\right)\right\}^T\left\{\mathbf{Z}_b\,(t) + r\left(x_{v_1}\right)\right\}\right] \\ & + k_{v_2}\left[z_v\,(t) + d_2\theta_v\,(t) - \left\{\mathbf{I}_b\left(x_{v_2}\right)\right\}^T\left\{\mathbf{Z}_b\,(t) + r\left(x_{v_2}\right)\right\}\right] \end{aligned} \tag{2}$$

$$\begin{aligned} 0 = {} & I_v\, \ddot{\theta}_v\,(t) \\ & + d_1 c_{v_1}\left[\dot{x}_v\,(t) + d_1\dot{\theta}_v\,(t) - \left\{\mathbf{I}_b\left(x_{v_1}\right)\right\}^T\left\{\dot{\mathbf{Z}}_b\,(t) + v r'\left(x_{v_1}\right)\right\}\right] \\ & + c_{v_2}\left[\dot{z}_v\,(t) + d_2\dot{\theta}_v\,(t) - \left\{\mathbf{I}_b(x_{v_2})\right\}^T\left\{\dot{\mathbf{Z}}_b\,(t) + v r'\left(x_{v_2}\right)\right\}\right] \\ & + k_{v_1}\left[z_v\,(t) + d_1\theta_v\,(t) - \left\{\mathbf{I}_b(x_{v_1})\right\}^T\left\{\mathbf{Z}_b\,(t) + r\left(x_{v_1}\right)\right\}\right] \\ & + k_{v_2}\left[z_v\,(t) + d_2\theta_v\,(t) - \left\{\mathbf{I}_b(x_{v_2})\right\}^T\left\{\mathbf{Z}_b\,(t) + r\left(x_{v_2}\right)\right\}\right] \end{aligned} \tag{3}$$

where $\mathbf{Z}_b\ (t) = \{Z_{b_1}(t), Z_{b_2}(t), \ldots, Z_{b_n}(t)\}$ is the vector of displacement each node from 1 to n_b on the bridge system. $\mathbf{l}_b(x_{v_1})$ designates the vector that contains polynomial interpolation functions for the displacement of the bridge system observed at the contact point of the ith axle. The over-dot and prime symbolize the derivative with respect to time and space, respectively.

The dynamic equation of motion of the bridge can be expressed in Equation (4) where mass, stiffness, and damping matrices $[\mathbf{M}_b]_{2n_b\times 2n_b}$, $[\mathbf{K}_b]_{2n_b\times 2n_b}$, $[\mathbf{C}_b]_{2n_b\times 2n_b}$ can be constructed from the bridge parameters.

$$\begin{aligned} & [\mathbf{M}_b]\left\{\ddot{\mathbf{Z}}_b\,(t)\right\} + [\mathbf{C}_b]\left\{\dot{\mathbf{Z}}_b\,(t)\right\} + [\mathbf{K}_b]\{\mathbf{Z}_b\,(t)\} \\ & \qquad + \left\{\mathbf{l}_b\left(x_{v_1}\right)\right\} R_1\,(t) + \left\{\mathbf{l}_b\left(x_{v_2}\right)\right\} R_2\ (t) = 0 \end{aligned} \tag{4}$$

where $R_1(t)$ and $R_2(t)$ are the contact forces at axle position x_{v_1} and x_{v_2}. The contact forces at each time step can be calculated at the time-step. The combination of all equations becomes a dynamic coupling equation that represents the whole vehicle–bridge system in Figure 1. The equation can be solved by Newmark-β method for implicit time integration. The method solves the displacement, velocity, and acceleration at $t + \Delta t$ from the current stage t and known information at $t + \Delta t$. The γ and β constant parameters of the Newmark-β method are 0.5 and 0.25, respectively.

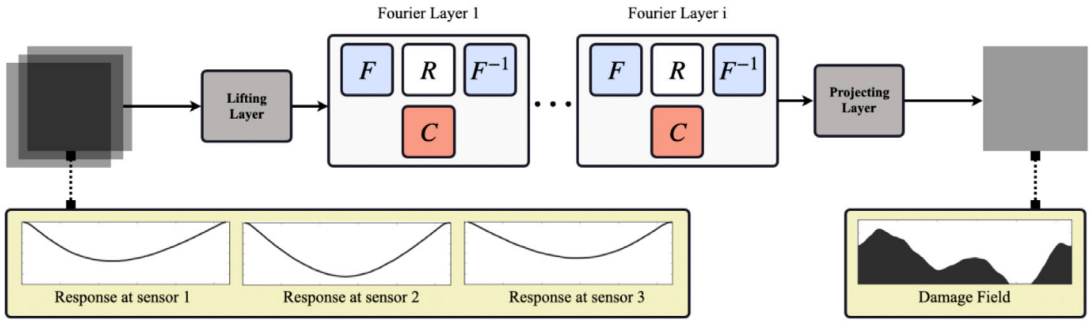

FIGURE 2 Fourier neural operator architecture in inverse problems, which is composed of three main parts: lifting, Fourier, and projecting layers. In a Fourier layer, the Fourier transform (F), linear transform with lower Fourier-mode filtering (R), inverse Fourier transform (F^{-1}), and convolution transform (C) are applied (Li et al., 2020). Herein for inverse problems, the inputs are structural response, and the output is the damage field.

2.2 | Fourier neural operator

T. Chen and Chen (1995) first proved the Universal Representation Theory of neural operators in 1995, that neural networks could be trained to fit arbitrary operators. Recently, neural operators have been rapidly developed to learn the mapping from the input field to the output field of partial differential equations (Kovachki et al., 2021). The architectures of the neural operator enhance the ability to map between functions with infinite-dimensional space (Kovachki et al., 2021; Li et al., 2020). FNO is a type of neural operator architecture that utilizes Fourier transform in the layers. FNO was reported to achieve the best performance among existing neural operators for solving complex partial differential equations as per Li et al. (2020). In this section, the framework and transfer learning for FNO are explained to be applied in the forward and inverse problems in SHM.

FNO architecture comprises three main components, which are lifting, iterative kernel operator, and projecting, as demonstrated in Figure 2. In the lifting section, the inputs of the model are lifted into the dimension of the iterative kernel operator through one fully connected or linear layer. After the dimensional trajectory shift, the iterative kernel operator is a branch of connected Fourier-layer blocks. The input in each block passes along two path functions. In the first path, the input undergoes a Fourier transform. Then, the linear layer (R in Figure 2) filters out high Fourier modes (higher than 16) before the inverse Fourier transform operates the data to another function. The first path can be expressed in Equation (7). In the second path, the input passes through a convolution layer. Subsequently, two paths merge to create layer output and become an input of the next layer. The last layer connects to the third part of the components—projection. The data are projected to the same dimension as the input to the model through two linear layers in the projection at the end of the architecture. Therefore, the inputs and outputs will always need to be the same dimensions.

In an iterative kernel operator, the integral operator in Equation (5) in neural operator was transformed into Fourier operator in Equation (6) as described in the FNO architecture based on the convolution theorem in Equation (7).

$$\left(K_t\left(\upsilon_t\right)\right)(x) \coloneqq \int_D \kappa(x,y)\,\upsilon_t(y)\,dy \tag{5}$$

$$\int_D \kappa(x-y)\,\upsilon_t(y)\,dy = F^{-1}\left(F\left(\kappa(x-y)\right) * F\left(\upsilon_t(y)\right)\right) \tag{6}$$

$$\left(K(\phi)\,\upsilon_t\right)(x) \coloneqq F^{-1}\left(R_\phi \cdot \left(F_{\upsilon_t}\right)\right)(x) \tag{7}$$

where κ is a kernel function. R_ϕ is the Fourier transform of a kernel function with periodic variation κ. R_ϕ is a written representation of a layer of neural network parameterized by ϕ and $R_\phi = F(\kappa)$; F and F^{-1} are defined as Fourier and inverse Fourier transform, written in Equation (8) and Equation (9).

$$\left(Ff\right)_j(k) = \int_D f_j(x)\,e^{-2i\pi\langle x,k\rangle}dx \tag{8}$$

$$\left(F^{-1}f\right)_j(x) = \int_D f_j(k)\,e^{2i\pi\langle x,k\rangle}dk \tag{9}$$

2.3 | Transfer learning

Transfer learning refers to a technique that utilizes the weights of a neural network or neural operator learned from an existing larger data set to a new unseen data set or to a similar problem. The approach not only reduced the training time on the new data set but benefited when the new data set was insufficiently large. Recent years have seen an increase in the application of transfer learning for

deep learning models in many fields. Fine-tuning is one of the transfer learning methods, which trains pretrained models on a new data set. Since the pretrained models usually consist of many layers, fine-tuning can be conducted in only some layers in the models; and typically, a few last layers are trained while the rest of the model is frozen (Chamangard et al., 2022; W. Chen et al., 2021; Reyes-Carmenaty & Pérez, 2022).

In civil engineering, transfer learning approaches have also been vastly adapted for the purposes of learning adoptions and reducing training time. Reyes-Carmenaty and Pérez (2022) utilized a computer vision-oriented pretrained model named ResNet34 and fine-tuned it on Complex Frequency Domain Assurance Criterion (CFDAC) matrix to detect alteration in stiffness. In addition, the CNN-based models such as VGG, ResNet, and AlexNet were mostly utilized in vision-based crack detection tasks as the models were pretrained on images (Wang et al., 2022). However, Chamangard et al. (2022) also applied CNN-based acceleration responses with transfer learning to obtain highly accurate damage detection on insufficient data. Although the data set was not big, the pretrained models were also fine-tuned with damage data on the Tianjin Yonghe Bridge at the detection level.

Transfer learning mostly uses in cases of limited data for a specific task. Therefore, in the BHM field, transfer learning will benefit when experimental data are limited. The numerical data could be used to train the model, then we can use experimental data to train the pretrained model as suggested in the framework of this paper. In this study, we trained a neural operator (VINO) to understand a relationship between a damage field and response fields for the numerical data set, in both forward and inverse meanings. Then, the trained model again learns the relationship between a damage field and response fields for the experimental data set. This is considered transfer learning in the context that the model used the knowledge learned from the numerical data set in the experimental data set, and boosted the performance of the model.

In VINO developed in this study, only the projection layers (i.e., the last two layers) of the pretrained FNO model were fine-tuned based on an experimental data set of the healthy bridge. The weights in the lifting and iterative kernel operator components were not fine-tuned. The fine-tuning data set was only the responses from the health bridge obtained from experimental data. In the last two layers of the architecture, a total of 8449 out of 549,633 parameters were trainable in VBI system. The fine-tuning approach is feasible for real-world structures because field vibration tests on the new bridge can be conducted to serve as a data set for fine-tuning, while future vibration responses of structures can be fed to FNO to detect damage distribution.

2.4 | The proposed framework

Figure 3 illustrates the proposed framework to use the VBI information to pretrain and fine-tune the FNO. The framework consists of two main stages, which are VBI-FE data set preparation (stage 1) and the machine learning approach (stage 2). As previously mentioned, stage 1 adopted the VBI-FE model to generate a data set of damage fields and structural response fields. Stage 2 focused on the model training, testing, fine-tuning, and validating where both VBI-FE and VBI-EXP data sets are used to train, verify, fine-tune, and validate the model. It is important to emphasize that in the framework, only the responses from the bridge at the healthy state were used to fine-tune in order to predict damages on the bridge at the damaged state in the same system of VBI. Additionally, this framework can serve both forward and inverse problems, depending on the inputs and outputs of the FNO model. In stage 2 of Figure 3, the inputs are the structural responses while the outputs are the damage field, which can be referred to as the inverse problem for BHM.

3 | DATA SET ACQUISITION

3.1 | Numerical simulation setup for VBI-FE data set

This section explains the setup of the simulation for training the VINO model. First, this section will explain the model parameters in numerical simulation based on the governing equations of VBI. Then, the generation of the data set for model training will be described by the variation of damage input to the numerical model.

3.1.1 | The numerical bridge model

The bridge parameters came from measurements and calculations on the laboratory bridge, summarized in Table 1. The parameters were obtained from the previous research of Kim et al. (2016). The Rayleigh Damping (c) is

TABLE 1 Bridge parameters.

Parameters	Values	Units
Speed	1.35	m/s
Space between axles	0.3	M
Sprung mass	15.38	kg
Suspension stiffness (axle 1 and axle 2)	1,666	N/m
Suspension damping (axle 1 and axle 2)	45.28	Ns/m

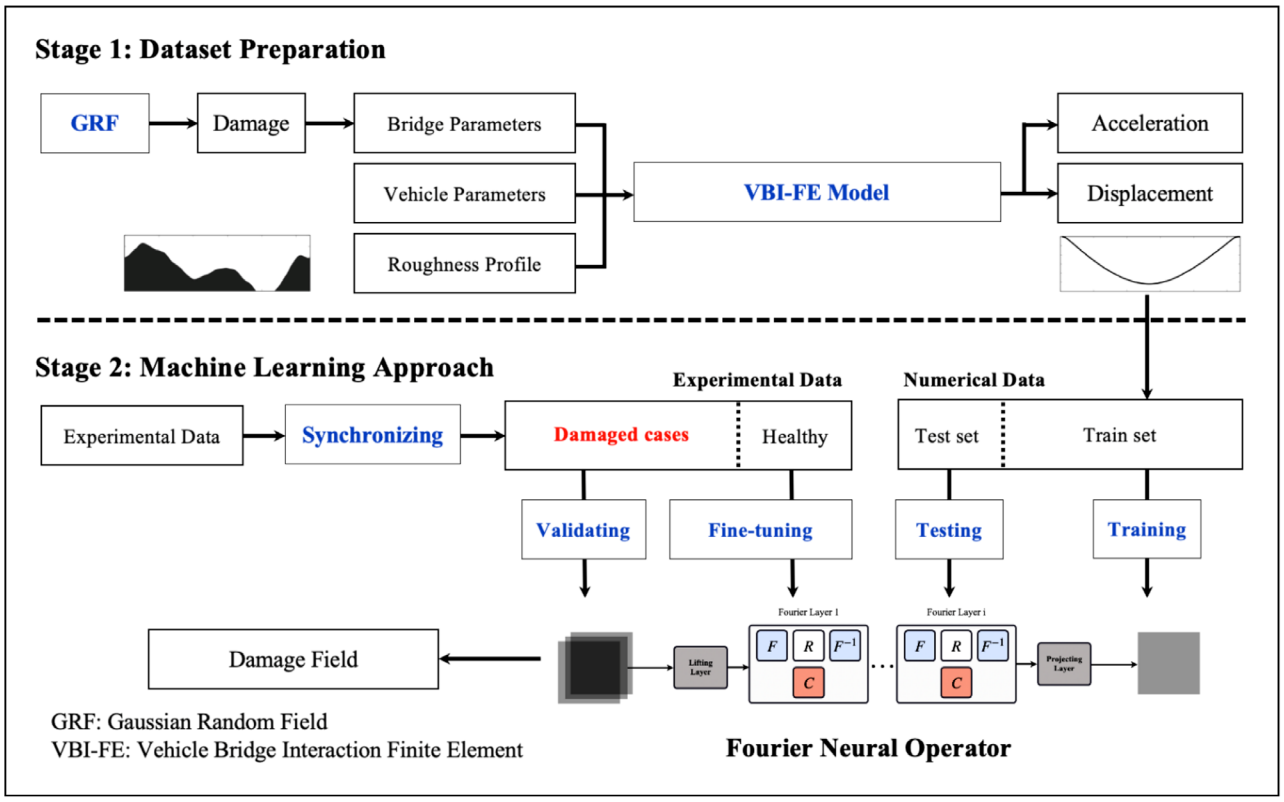

FIGURE 3 The overall proposed data-driven framework and procedures.

written in the form of fractions of mass (M) and stiffness (K) with two coefficients as shown in Equation (10). The mass coefficient (α_{dM}) and the stiffness coefficient (β_{dK}) are formulated based on the first and second frequency and damping ratios.

$$c = \alpha_{dM} M + \beta_{dK} K \tag{10}$$

where the damping ratios are equal to 0.007 according to the in-house experiment described in Section 3.2.

3.1.2 | The numerical vehicle model

The half-car model is adopted to simulate the VBI system. Table 2 summarized the parameters of the vehicle measured in the in-house experiment. The speed of the vehicle on the laboratory bridge ($v = 0.55$ m/s) is equivalently converted to the vehicle speed on the real bridge ($v = 10$ km/h), using the speed parameter shown in Equation (11). It is noted that the equivalent vehicle weight is 18,000 kg. The equivalent vehicle length is 2.4 m.

$$\gamma = \frac{v}{2 \cdot f_1 \cdot L} \tag{11}$$

where γ denotes the speed parameter; v refers to the speed of the vehicle on the bridge with the first mode frequency (f_1) and length (L).

TABLE 2 Vehicle parameters.

Parameters	Values	Units
Element	512	
Length	5.4	m
Mass per unit length	53.47	kg/m
Young's modulus	2.1×10^{11}	Pa
Moment of inertia	5.49×10^{-7}	m^4
Frequencies (1st and 2nd modes)	3.64, 14.56	Hz
Rayleigh damping coefficient (α_{dM}, β_{dK})	0.2562, 1.22×10^{-4}	1/s,s

Moreover, suspension damping was calculated based on the mass and stiffness of the vehicle.

$$c = c_c \times \zeta_v \tag{12}$$

where ζ_v is the damping ratio obtained from free vibration tests of the same bridge (Cantero et al., 2019; McGetrick et al., 2015). c_c indicates the critical damping, which equals to $2\sqrt{m_a k_a}$. In the calculation, the mass of each axle (m_a) was assumed to be half of the total mass of the vehicle (m_v). Thus, the damping ratio of the two axles was 45.28 Ns/m.

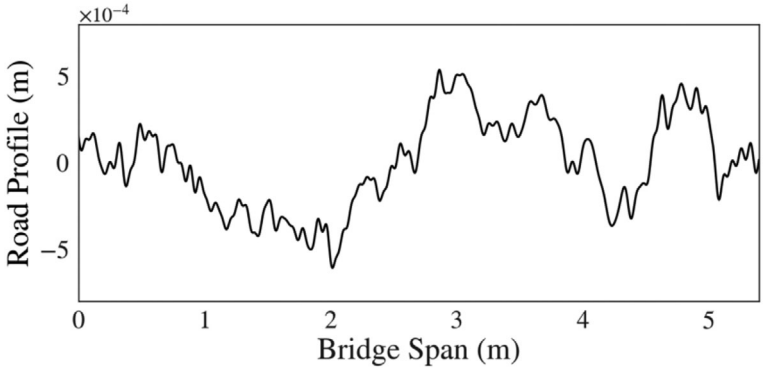

FIGURE 4 Road profile on the laboratory bridge.

3.1.3 | The road profile

The road irregularity profile was obtained from measurements under a path of a tyre on the experimental bridge, plotted in Figure 4. As classifying the roadway roughness using the Power Spectral Density (PSD) of the roadway roughness based on ISO 8608, a condition of a roughness profile is representative of the entire bridge width (ISO 8608, 2016).

3.1.4 | The numerical VBI-FE data set

The data set stands as the most influential component in the machine learning model. In damage detection, data sets must be considered and prepared as carefully as possible regarding accuracy and practicality. Since in machine learning application research, the models are trained on the training set and tested on the testing set, it is always possible that a training set does not provide the coverage of all possible cases, resulting in an impractical model.

In VINO, FE simulation of a VBI system is first adopted to generate a numerical data set VBI-FE based on the random damage possibility of every element on the 512-sectioned bridge. The Gaussian random field is utilized to generate continuous random damage fields according to the distribution field,

$$N\left(\mu, \sigma^2\left[(-\Delta + \tau^2 I)\right]^{-\gamma}\right)$$

where the mean (μ) is 0.2, the variance (σ^2) is 49, the nugget effect (τ) is 7, and the scaled parameter (γ) is 2.5 for the data set generation. Furthermore, the range of random distribution was from 0% to 95% of stiffness reduction to ensure the physical meaning of the obtained damage field. The random continuous stiffness reduction or damage level for each element, thus, generates a random damage field.

The data set was prepared from simulation runs in MATLAB software on the computer spec Intel(R) Core(TM) i9-10850K CPU @3.6 GHz with NVIDIA GeForce RTX 3090 at the laboratory within 24 h with a single CPU thread. In total, the training and testing sets of VBI-FE include 1200 independent FE simulations. This study obtained the acceleration of all 514 nodes of bridge elements and the vehicle for 844 time steps in the VBI-FE data set. Then the data set was divided into 1000 and 200 simulations of responses for training and testing the FNO, respectively.

3.2 | Experimental setup for VBI-EXP data set

The actual experiments were conducted in the laboratory at Kyoto University to collect real-world data in order to provide validation and justification to the FNO models in both forward and inverse problems. The model bridge and model vehicle are measured and calculated for physical properties as the same values in Tables 1 and 2.

As schematically illustrated in Figure 5, the model bridge has an I-section, and the weak axis is loaded in the test. The total span length is 5.4 m. The boundary conditions of the bridge are the pin and roller supports on two ends. DMG1 (on the right) and DMG2 (on the left) were depicted in the schematic view in Figures 5a and 5b (Yokoyama et al., 2022). In this paper, the detachable reinforcements for DMG1 in Figure 5d and DMG2 in Figure 5e were considered as no damage. The bridge with two reinforcements is an intact case (INT), and the removal of reinforcement refers to a specific damage case. All scenarios are conducted on one bridge specimen, and DMG1 and DMG2 were estimated to be 16% and 13% reduction of the flexural rigidity by stiffness calculations. As previously mentioned, four damage scenarios (INT, DMG1, DMG2, and DMG3) were assumed and corresponded to intact, damage 1, damage 2, and damage 3 conditions, whereas DMG3 is the combination of the existence of DMG1 and DMG2.

The dynamic response data of the bridge were collected from sensors placed on and under the bridge. The actual setup is shown in Figure 5c where three displacement transducers (CDP-50 mm) and three wired accelerometers

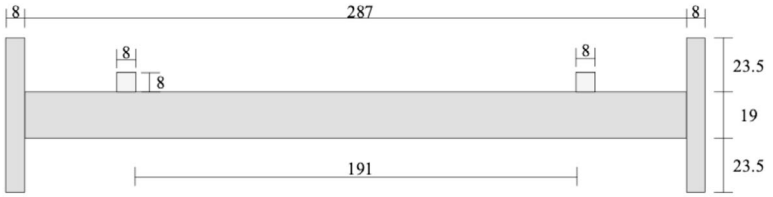

(a) Cross-sectional design of the laboratory bridge (Yokoyama et al. 2022)

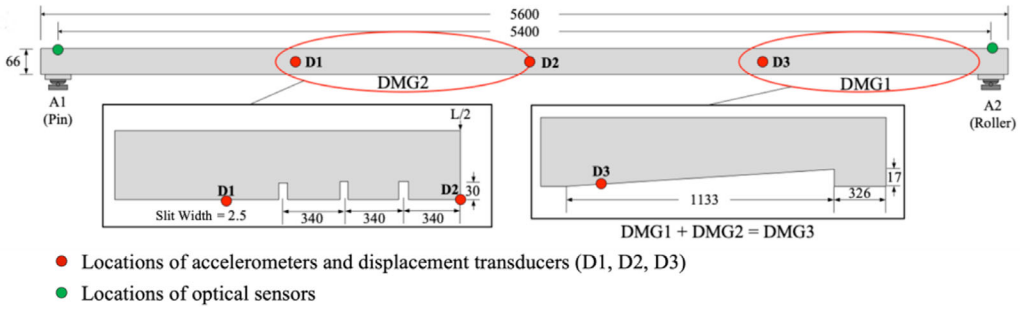

(b) Schematic design of the laboratory bridge (Yokoyama et al. 2022). Three displacement transducers and wired accelerometers were placed at quarter (D1), mid (D2), and three-quarter (D3) spans.

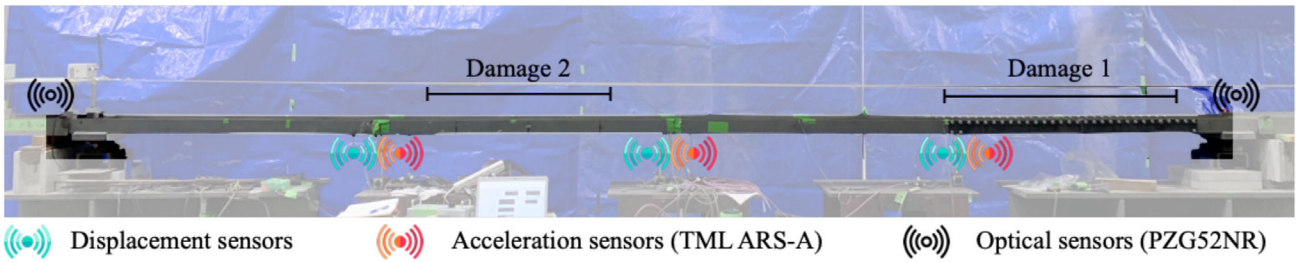

(c) The experimental bridge

(d) The reinforcement at DMG1

(e) The reinforcement at DMG2

(f) The experimental bridge without a reinforcement (DMG1)

(g) The experimental bridge without a reinforcement (DMG2)

FIGURE 5 Experimental setups.

(M-A552AC10) were installed at the quarter, mid, and three-quarter spans along the bridge. Two optical sensors (NPN PZ-G52N) were located at two ends in order to track the entry and exit of the vehicle in the system. The details of the vehicle were summarized in Table 2. Two wireless accelerometers were also attached on top of the vehicle to monitor the acceleration of the vehicle during the experiment. All sensors were connected to the central control panel, namely, DC-7204 Dynamic Strain Recorder measurement software. A small triggering force was applied to the bridge to asynchronously set the start of one testing round for all sensors and transducers for data processing.

4 | PERFORMANCE OF VINO ON VBI-FE NUMERICAL DATA SET

This section provides the numerical verification of VINO for forward and inverse problems. As shown in the framework of Figure 3, the numerical data set was divided

into the training set and testing set. In this section, the performance of VINO on the testing set is reported to discuss the efficiency of the VINO. For the structural simulation problem, the forward VINO aims to generate structural responses from the input of a particular damage distribution curve, which is similar to FE simulation. For the SHM problem, the inverse VINO is validated by the accuracy in predicting damage fields from the structural responses at several sensor locations.

4.1 | Forward VINO for structural simulation

Structural simulation is considered a forward problem due to the fact that it solves differential equations to obtain the responses of bridge and vehicle. The conventional model applies the FE method, as explained in Section 2.1, and the proposed VINO model is a data-driven architecture that learns from the VBI-FE data set.

VINO and the FE model should be compared to assess which is more effective, taking into account errors and computational time. Therefore, this verification aims to discuss a more efficient model for further forward problem purposes. This paper provided numerical verification for VINO models trained to generate displacement, rotational angle, and acceleration from a random damage field in Figure 6.

To obtain displacement response, VINO was trained to predict a single channel of displacement measurement data. Therefore, three VINO models were trained to capture the response from three locations (1/4 span, mid-span, and 3/4 span). After being trained on the 1000 training data in the VBI-FE data set, VINO models are capable of generating the same output as the FE simulation results. Figure 6a shows the damage field input to both models, while responses in Figure 6b are the output of the models. In Figure 6a, damage level is the percentage of stiffness reduction at each element. As observed in Figure 6b, each displacement response was obtained from each VINO with an error below 40 μm. In addition, the FE simulation time is 66 s to obtain response at 1028 nodes on average based on a single core of Intel(R) Core(TM) i9-10850K CPU @3.6 GHz with NVIDIA GeForce RTX 3090. In comparison, after the training process is complete, the inference time of VINO is only 3.4 *ms* to obtain one response based on a single Nvidia V100 GPU. This implies that for the full simulations, FNO will be 19 times faster than the FE model once it is trained. For a specific task that requires only selected nodes, VINO will achieve notably higher computational efficiency in structural response prediction because of the efficient utilization of parallel computing resources of GPU accelerators, and there is no need to form a stiffness matrix or matrix solver in VINO. Therefore, the result can be concluded for the excellent performance of the VINO in learning to map the damage field to the displacement at an arbitrary node, which is at least as accurate as the FE model. It is noted that the training is specific to a data set of a road profile, a response type, a vehicle type, and a bridge type.

Figure 6c shows the performance of VINO in fitting the rotation angle of the bridge. Similar to the displacement responses, the rotational angles of bridge responses from VINO were considerably close to those obtained from the FE model. The maximum error of rotation angle is less than 10^{-5} degrees observed at the bottom of Figure 6c. The inference time of VINO is similar to that of the displacement prediction model and is notably faster than the FE model. This suggests that VINO could reproduce FE simulation results of rotational angle.

The acceleration response data vary and fluctuate over time domain and are more sensitive to FE modeling parameters such as damping ratio. In Figure 6d, the acceleration responses of the quarter-span generated from VINO and FE simulation were shown. Although higher errors were observed in acceleration prediction, the general trend of acceleration obtained from FE simulation is replicated by the VINO model. The error between VINO and FE simulation was lower than 1 mm $\cdot$ s^{-2}. After the training process is complete, like displacement and rotational angle, the acceleration response at each node was inferred within 3.5 ms, suggesting a higher efficiency than the FE model. The Fourier mode in the Fourier layers of VINO was 16 as applied to approximate the one-dimensional field in Li et al. (2020), which was discussed to be sufficient in the approximation. Although the current progress of this study does not aim to investigate the most efficient Fourier mode, it should be noted that an analysis of the Fourier mode may be needed to optimize the computational time and accuracy.

As a result, all three numerical verifications concluded that VINO has the competence to simulate the deflection, rotational angle, and acceleration responses as the FE model created in the forward problem at the quarter, mid, and three-quarter span locations. This further suggests the ability to generate other structural responses of the other nodes on the bridge in the data set. From the results, an apparent advantage of the VINO over the FE simulation is the inference time, which is almost 2000% faster than the FE model for a full simulation. Another suggestion for the full operation is the two-dimensional VINO to predict the displacement field as a function of coordinate (x) and time (t), which should be investigated for applications in forward VBI problems. It is believed that if the two-dimensional model provides high accuracy, it can be a great benefit to future VBI research.

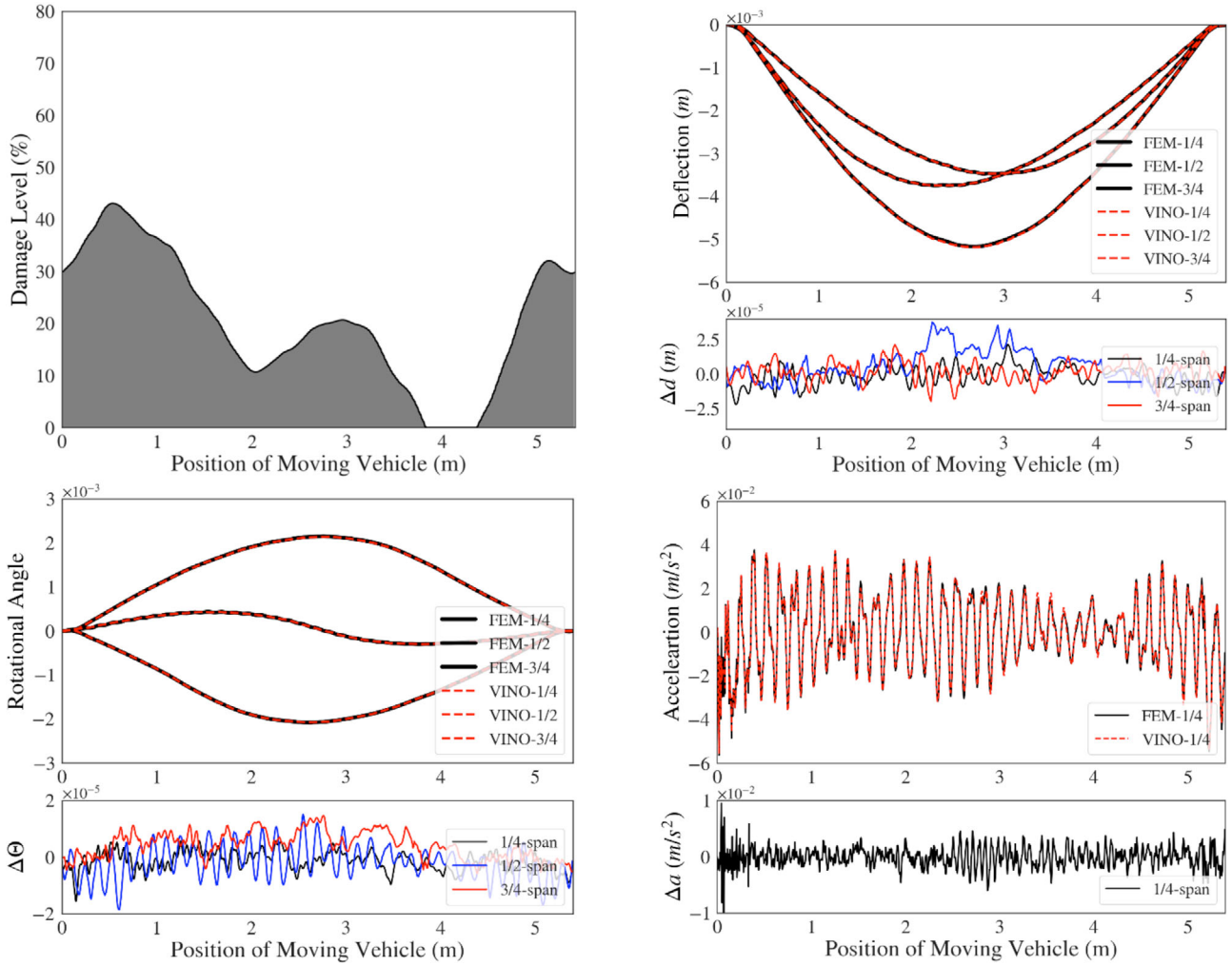

FIGURE 6 Numerical results of Vehicle–Bridge Interaction Neural Operator (VINO) on the forward problem. (a) Damage field input, which represents damage level or the stiffness reduction at each position on the bridge; (b) deflection responses and their differences between two models; (c) rotational angle responses and their differences between two models; (d) acceleration responses and their differences between two models.

4.2 | Inverse VINO for SHM

As mentioned in Section 1, damage detection in BHM is considered an inverse problem because the approach aims to find the causal parameter (damage distribution) from the detected vibration responses. In this case, the damage on the bridge is the parameter that causes the difference in the measurement of structural responses. This section presents the results of the VINO that maps from the structural responses field to the damage field. The inputs of VINO are structural responses at the quarter, mid, and three-quarter spans on a numerical bridge, and the output is the damage field. In this paper, only two responses, as shown in Figure 7—displacement and accelerations—were investigated because these can be easily measured with displacement sensors and accelerometers.

To predict damage fields from displacement responses, the VINO was trained, in which the inputs were an array of the displacement responses (Figure 7a) at three nodes, including quarter, half, and three-quarter spans, and the output was the damage field (Figure 7b). In Figure 7b, the black line depicts the theoretical damage field, which is an input to the FE model to generate the structural responses, and the red line represents the damage field predicted by VINO. Therefore, numerical results from Figure 7b showed the considerably accurate prediction of VINO in mapping between displacement and damage fields, suggesting the capability to predict damage along the bridge span. The inaccurate prediction can be seen at the bridge's start and end because the structural response is not sensitive to the possible damage at the beam end.

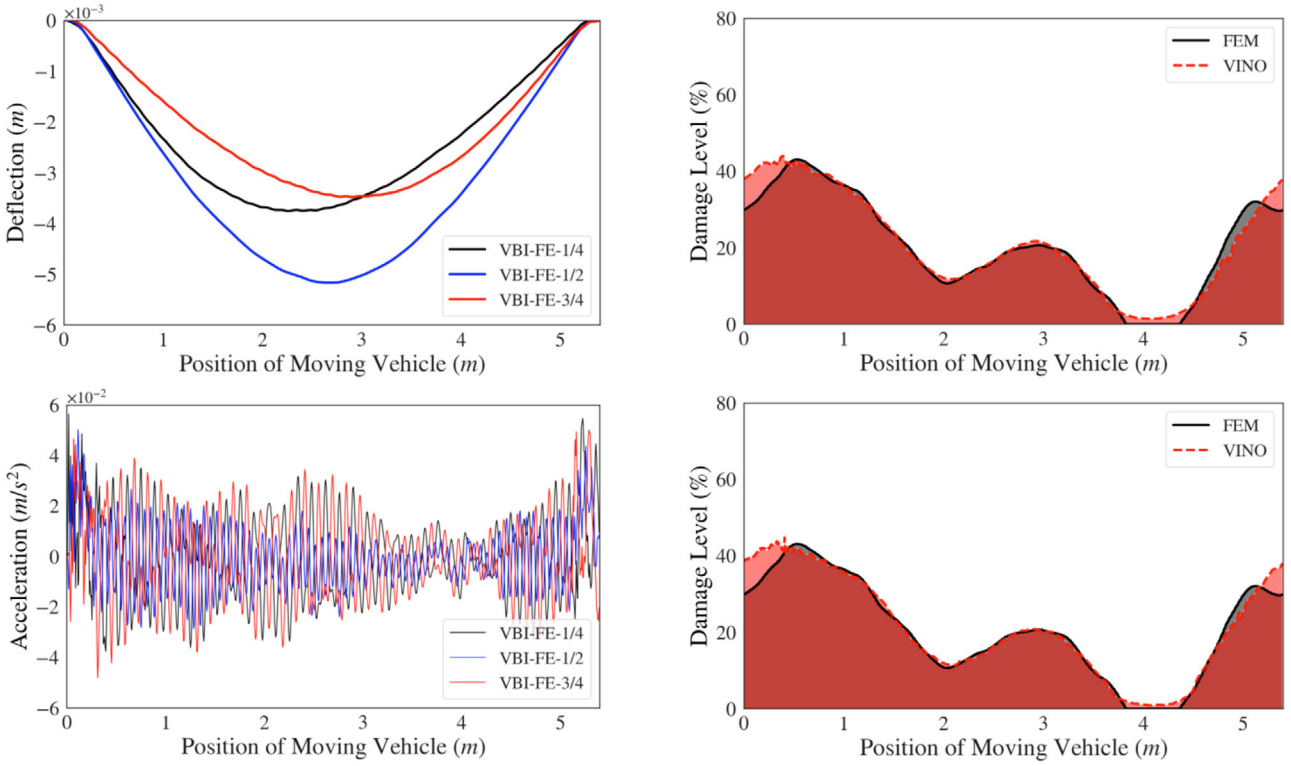

FIGURE 7 Numerical results of Vehicle–Bridge Interaction Neural Operator (VINO) on the inverse problem. (a) Deflection responses at the quarter, half, and three-quarter span; (b) theoretical and predicted damage fields by VINO; (c) acceleration responses at the quarter, half, and three-quarter span; (d) theoretical and predicted damage fields by VINO.

Although acceleration responses have more high-frequency components compared to the deflection, as shown in Figure 7c, the damage fields in Figure 7d predicted by VINO trained by the acceleration inputs showed results similar to the damage fields predicted from the displacement inputs. Three acceleration responses at the quarter, mid, and three-quarter nodes were the inputs of the VINO model, which was able to predict an accurate damage field in the numerical verification. This suggested investigations of VINO for the experimental data with only sensors at the three locations.

Observations from the simulation data–based investigation demonstrated that it is sufficient to draw a conclusion that VINO is an excellent candidate in damage detection for determination, localization, and quantification. Because the encoder-based architecture maps between two function spaces, the machine learning model can predict the damage field from displacement or acceleration responses discussed above in Figure 7. Similar to several other research, these numerical verifications, in fact, do not provide sufficient justification for the practicality of the model. To overcome the challenges of data-driven SHM mentioned in review articles (Avci et al., 2021; Azimi et al., 2020; Gordan et al., 2022; Malekloo et al., 2021; Toh & Park, 2020), the numerically verified FNO will be validated with the experimental data in Section 5 as mentioned in the framework (Figure 3). In addition, it is believed that the one-dimensional FNO suits better with this inverse problem in comparison to the two-dimensional FNO because the inputs can be detected responses from as many sensors as necessary and the output is a damage field, which is strictly one dimension. However, if the problem goes up to the three-dimensional structure, it is suggested to further develop the higher dimensional VINO models.

5 | PERFORMANCE OF FINE-TUNED VINO ON THE VBI-EXP DATA SET

In this section, the experimental validation for VINO was reported for both forward and inverse problems. In the forward problem of structural simulation, this validation aims to provide a justification that after transfer learning, VINO can generate more reliable structural responses than the conventional FE model. For the inverse problem, validation is provided to demonstrate data-driven BHM.

During the fine-tuning process, we obtained the dynamic responses of the intact case (INT), in which the damage level of the dynamic responses is expected to be zero along the damage field. Then, we train the pretrained VINO to obtain the zero along the damage field, which is now called fine-tuning. After that, the fine-tuned VINO

is tested with dynamic responses of DMG1, DMG2, and DMG3 and compared for the results.

To approach those goals as a practical approach in the forward and inverse problems, the model must be validated by the data of the actual bridge at the damage state (not the numerical data) in which the model is making a prediction. This means the model will be pretrained on the VBI-FE data set and fine-tuned on the VBI-EXP data set or the real experimental data from the bridge only at the healthy state by transfer learning. Subsequently, VINO can predict the damage fields on the bridge when the damages appear.

5.1 | Fine-tuned forward VINO for structural simulation

In VBI problems, it is still a challenging problem to generate the exact responses as the experiments, even though the numerical and experimental setups are identical due to the fact that the numerical models (FE method) have some assumptions (elastic material, Rayleigh damping model, etc.). In machine learning–based approaches, transfer learning approaches are applied to a model to utilize an understanding of the pattern or function of a specific task.

In the structural simulation problems, the forward VINO was fine-tuned to simulate displacement responses only. After the VINO model was pretrained on the VBI-FE data set of 1000 simulations and validated in Section 4, it was then fine-tuned on the VBI-EXP data set obtained from experiments on the laboratory bridge. As mentioned in previous sections, only the responses from the bridge at the healthy state (INT scenario) were adopted to train the last two layers of the VINO model, while other layers in the model were frozen. After that, the fine-tuned VINO model was further validated by three damage scenarios as prepared in the VBI-EXP data set: DMG1, DMG2, and DMG3 as reported in the experimental setup in Section 3.1.

Figure 8 showed the comparison between the collected experimental data in the VBI-EXP data set, FE simulation, and the VINO model trained on the VBI-FE data set and fine-tuned on the VBI-EXP data set in simulating the displacement responses of the bridge. Figure 8a is the result on the healthy bridge (i.e., training set in the VBI-EXP data set). The difference between the actual experimental responses and the FE model of the healthy bridge is around 1.25 mm at the maximum experimental displacement (3.4 mm), equivalent to a relative error of 37%. However, the error between the VINO and experimental results is approximately 0.3 mm along the response field. As the pretrained VINO was fine-tuned with the INT scenario, a small error was expected. A similar trend was shown in Figure 8b for the DMG1 scenario. Compared to experimental data, the FE model and VINO showed maximum errors of nearly 1.1 mm and 0.5 mm, respectively. The performance of the FE model for simulating displacement responses under DMG2 and DMG3 in Figure 8c and d showed a larger error compared to VINO. The maximum error of the FE model was still above 0.65 mm along the displacement responses. In comparison, the fine-tuned VINO model reduced the displacement error to less than 0.55 mm along the span of the bridge. It is evident in DMG1, DMG2, and DMG3 that it was difficult for VINO to predict the response at the start and the end as the error was always one of the largest errors along the span. This error may come from the data processing during the synchronization of optical and three displacement sensors.

Therefore, it is concluded that the fine-tuned VINO showed better performance compared to the FE model in the forward problem (i.e., structural simulation problem). The maximum error between test and simulation results was reduced in VINO, and the oscillation of the actual displacement responses was also predicted by the VINO model. This may be attributed to the Rayleigh damping model adopted in FE simulation, which may dampen out high-frequency responses beyond the second frequency of the bridge structure. The fine-tuned VINO model was able to generate high-frequency component displacement responses, as shown in Figure 8.

5.2 | Fine-tuned inverse VINO for SHM

The transfer learning of the inverse problem for BHM shows the practical application of VINO. In this section, the validation will be reported to illustrate that the proposed model VINO is able to predict DMG1, DMG2, and DMG3 after conducting the fine-tuning approach only with responses of the healthy bridge in the VBI-EXP data set. In this paper, both displacement and acceleration responses at the 1/4-span, mid-span, and 3/4-span are used to investigate the practical application of the VINO with displacement data or acceleration data.

Figure 9 shows the experimental deflection curve measured by displacement sensors and the predicted damage distribution of VINO compared to the theoretical damage distribution. Figure 9 clearly demonstrates that VINO is capable of predicting all the expected damage scenarios on the laboratory bridge. In the training set, the damaged responses did not appear after fine-tuning. In the test set, the model understood damage 1 and 2 in the DMG1 and DMG2 scenarios. VINO predicts the accurate combination of damage 1 and 2 in damage 3 of the DMG3 scenario. The small damages in Figure 9b, d, f, and h are considered the errors at the current stage as they are considerably small

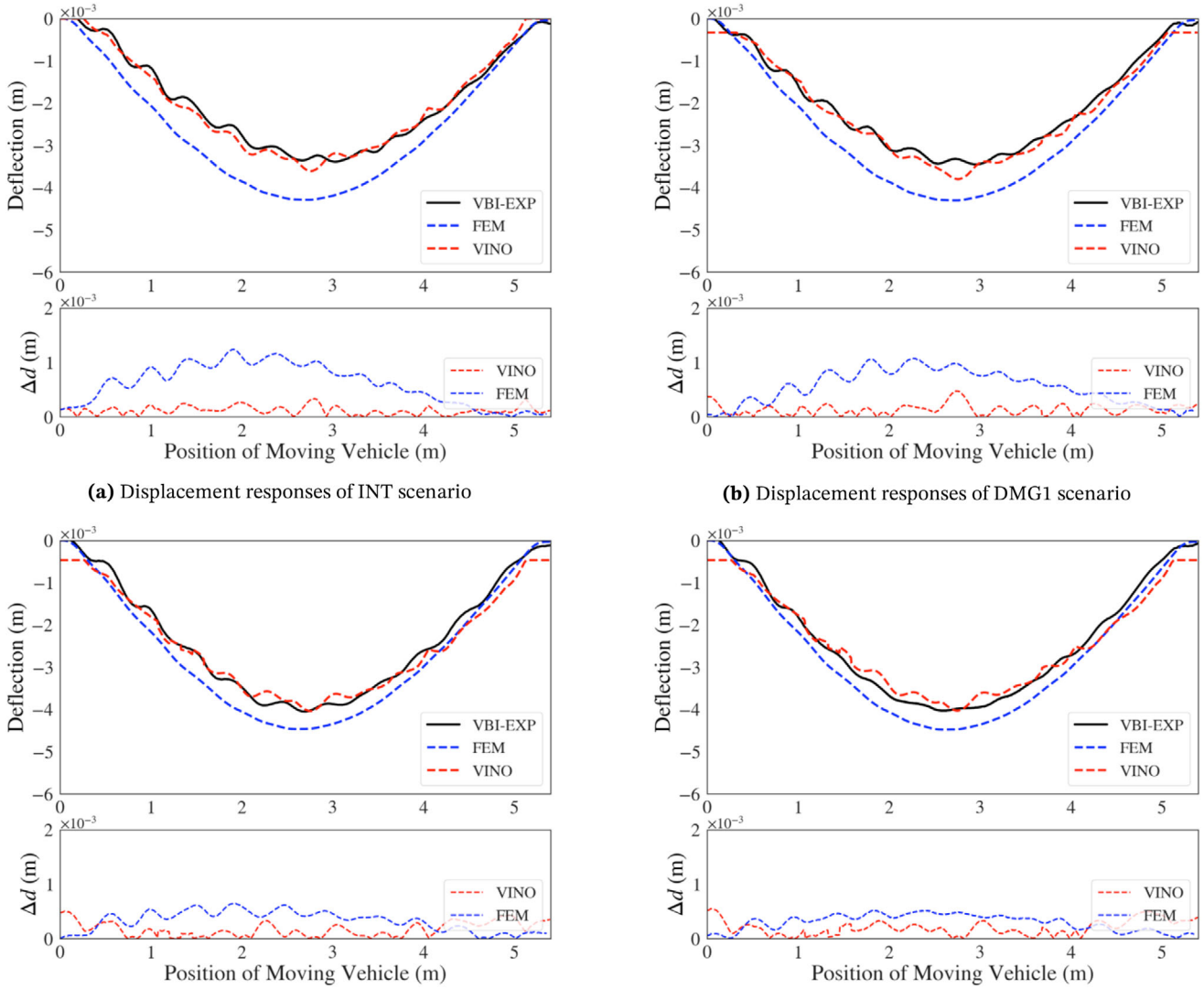

(a) Displacement responses of INT scenario

(b) Displacement responses of DMG1 scenario

(c) Displacement responses of DMG2 scenario

(d) Displacement responses of DMG3 scenario

FIGURE 8 Experimental validation of Fourier neural operator on the forward problem. This compares the deflection responses of (a) INT, (b) DMG1, (c) DMG2, and (d) DMG3 scenarios.

(less than 5%) compared to the expected damage (over 15%). In addition, as observed in the figures, the spatial resolution of the damage field of VINO cannot precisely obtain the real damage field, which may be attributed to the limited number of sensors in this study. This could be the effect of both the sensors and the limited size of the training set in the VBI-FE data set, where the damage distribution generated was very smooth, and this particular shape of damage as a piecewise function was not observed. However, the results can determine the excellent performance of VINO.

For the acceleration responses, the results of the investigation are shown in Figure 10. The accelerations in the time domain include high-frequency signals. Compared to the VINO trained by displacement data, the fine-tuned VINO achieved prediction of the damage field with higher errors as shown in Figure 10b, d, f, and h. It was observed that the VINO model for acceleration was able to predict damage 1, damage 2, and damage 3 in the DMG1, DMG2, and DMG3 scenarios to a certain level. The predictions of DMG1 and DMG2 were better than that of DMG3. The main source of error may originate from a larger noise of the signal. This suggested conducting further studies to obtain a larger experimental data set for fine-tuning VINO models. Compared to conventional FE model updating algorithms in BHM in the time domain or frequency domain conducted by Lin et al. (2021), VINO achieved end-to-end damage detection without the need for model updating, which notably reduced the time in damage detection.

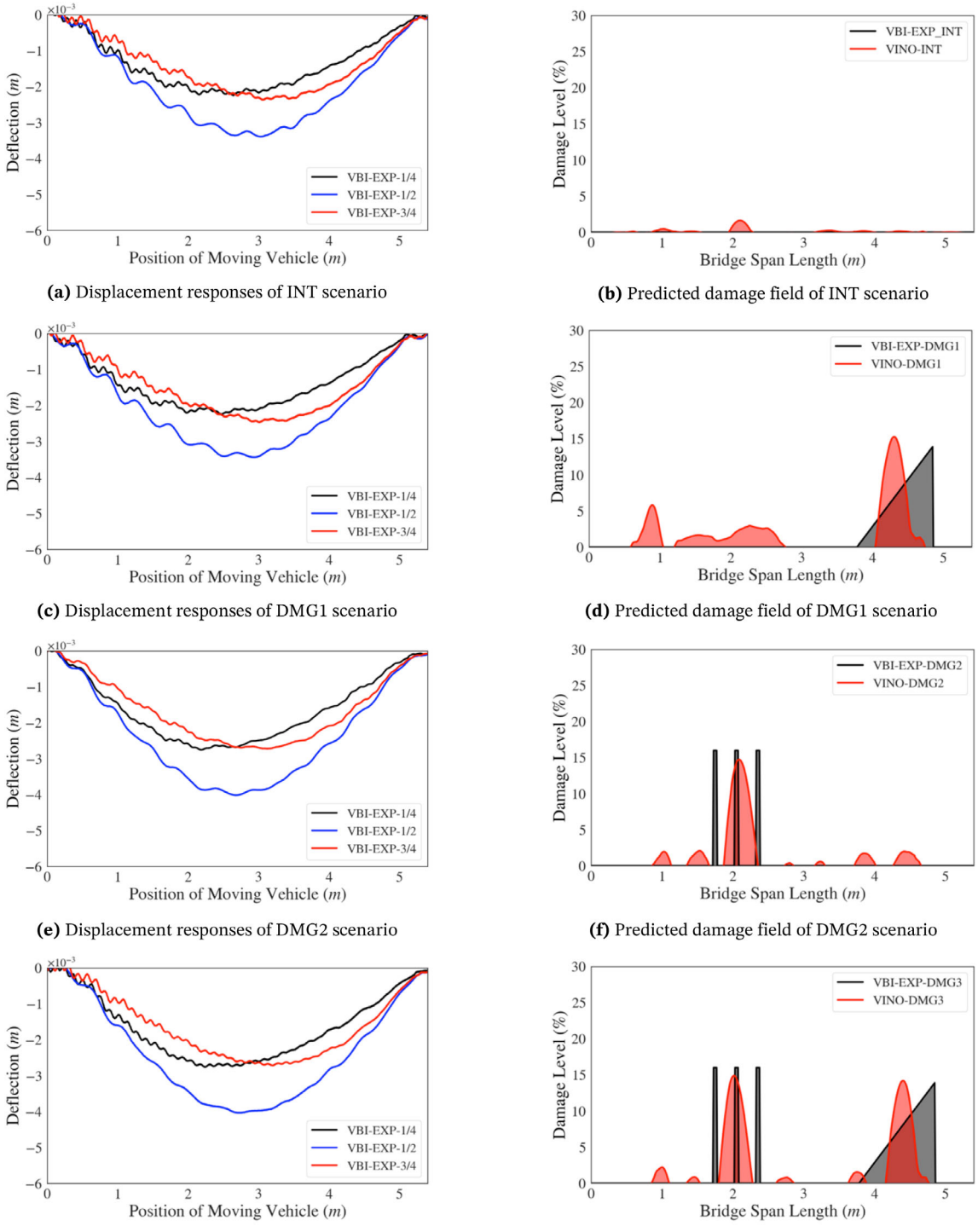

(a) Displacement responses of INT scenario

(b) Predicted damage field of INT scenario

(c) Displacement responses of DMG1 scenario

(d) Predicted damage field of DMG1 scenario

(e) Displacement responses of DMG2 scenario

(f) Predicted damage field of DMG2 scenario

(g) Displacement responses of DMG3 scenario

(h) Predicted damage field of DMG3 scenario

FIGURE 9 Experimental validation of fine-tuned inverse Vehicle–Bridge Interaction Neural Operator (VINO) for structural health monitoring. These are comparison of predicted damage fields for INT, DMG1, DMG2, and DMG3 scenarios from displacement fields.

6 | CONCLUSION

This paper proposed the VINO framework that can serve as a surrogate model of bridge structures with the VBI effect. Learning function mappings from VBI-FE and VBI-EXP data sets, the VINO framework contributes to the following breakthroughs of data-driven SHM.

1. VINO model is end-to-end, fast, and accurate in forward (structural simulation) and inverse (SHM) problems.

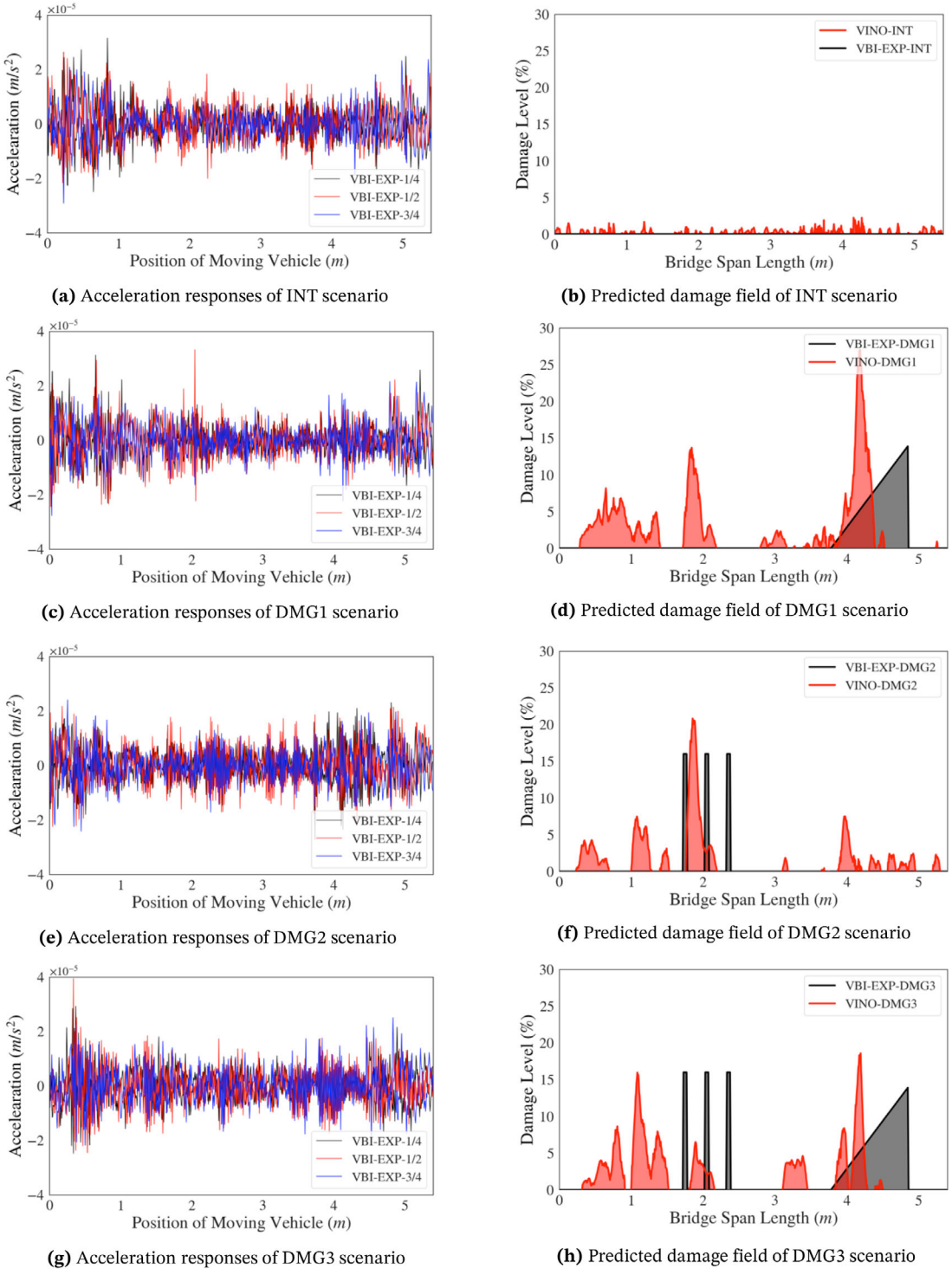

(a) Acceleration responses of INT scenario

(b) Predicted damage field of INT scenario

(c) Acceleration responses of DMG1 scenario

(d) Predicted damage field of DMG1 scenario

(e) Acceleration responses of DMG2 scenario

(f) Predicted damage field of DMG2 scenario

(g) Acceleration responses of DMG3 scenario

(h) Predicted damage field of DMG3 scenario

FIGURE 10 Experimental validation of fine-tuned inverse Vehicle–Bridge Interaction Neural Operator (VINO) for structural health monitoring. These are comparisons of predicted damage fields for INT, DMG1, DMG2, and DMG3 scenarios from acceleration fields.

2. For the forward problem, the FE simulation results of bridge response can be captured by the VINO model with over 19x faster inference speeds.
3. For the forward problem, after fine-tuning from the healthy bridge data, the VINO achieved better displacement response prediction of a structure compared to FE simulation results.
4. For the inverse problem, the VINO model can achieve the all-in-one damage determination, localization, and quantification model.

5. For the inverse problem, the VINO model, which was fine-tuned from the healthy bridge data, efficiently predicted damages on the test bridge.

While the VINO model showed remarkable results, the limitations of the model include three conditions. First, the VINO model requires establishing numerical and experimental data sets as there is a strong need to develop high-fidelity data sets to train state-of-the-art models. Second, more parameters may need to be added to VINO architecture for more generalization in the application. Third, the current VINO model is a data-driven approach. More physics constraints can be added to VINO to achieve physics-informed neural networks in the future. This may improve the performance of VINO and reduce the requirement for a big data set.

ACKNOWLEDGMENTS

This study is supported by the JSPS Fellowship (P22062), JSPS bilateral joint research projects (grant number JPJSBP120217405), The University of Hong Kong Start-up Fund for New Staff and The University of Hong Kong Seed Fund for Basic Research for New Staff, which are greatly appreciated.

REFERENCES

Abeykoon, D., Jayasinghe, J., & Dharmasiri, K. (2018). Damping change-based damage detection of PC bridges. In *The 7th Asia conference on earth-quake engineering*, November 22–25, 2018, Bangkok, Thailand.

Adeli, H., & Kim, H. (2001). Cost optimization of composite floors using neural dynamics model. *Communications in Numerical Methods in Engineering*, *17*(11), 771–787. https://doi.org/10.1002/cnm.448

An, Y., Chatzi, E., Sim, S.-H., Laflamme, S., Blachowski, B., & Ou, J. (2019). Recent progress and future trends on damage identification methods for bridge structures. *Structural Control and Health Monitoring*, *26*(10), e2416. https://doi.org/10.1002/stc.2416

Avci, O., Abdeljaber, O., Kiranyaz, S., Hussein, M., Gabbouj, M., & Inman, D. J. (2021). A review of vibration-based damage detection in civil structures: From traditional methods to machine learning and deep learning applications. *Mechanical Systems and Signal Processing*, *147*, 107077. https://doi.org/10.1016/j.ymssp.2020.107077

Azimi, M., Eslamlou, A., & Pekcan, G. (2020). Data-driven structural health monitoring and damage detection through deep learning: State-of-the-art review. *Sensors*, *20*(10), 2778. https://doi.org/10.3390/s20102778

Bao, Y., Tang, Z., Li, H., & Zhang, Y. (2019). Computer vision and deep learning–based data anomaly detection method for structural health monitoring. *Structural Health Monitoring*, *18*(2), 401–421. https://doi.org/10.1177/1475921718757405

Brownjohn, J. M. W. (2006). Structural health monitoring of civil infrastructure. *Philosophical Transactions of the Royal Society A: Mathematical, Physical and Engineering Sciences*, *365*(1851), 589–622. https://doi.org/10.1098/rsta.2006.1925

Cantero, D., McGetrick, P., Kim, C.-W., & OBrien, E. (2019). Experimental monitoring of bridge frequency evolution during the passage of vehicles with different suspension properties. *Engineering Structures*, *187*, 209. https://doi.org/10.1016/j.engstruct.2019.02.065

Cao, M., Sha, G., Gao, Y., & Ostachowicz, W. (2017). Structural damage identification using damping: A compendium of uses and features. *Smart Materials and Structures*, *26*, 043001. https://doi.org/10.1088/1361-665x/aa550a

Chamangard, M., Amiri, G., Darvishan, E., & Rastin, Z. (2022). Transfer learning for CNN-based damage detection in civil structures with insufficient data. *Shock and Vibration*, *2022*, 1–14. https://doi.org/10.1155/2022/3635116

Chang, K. C., & Kim, C. W. (2016). Modal-parameter identification and vibration-based damage detection of a damaged steel truss bridge. *Engineering Structures*, *122*, 156–173. https://doi.org/10.1016/j.engstruct.2016.04.057

Chen, T., & Chen, H. (1995). Universal approximation to nonlinear operators by neural networks with arbitrary activation functions and its application to dynamical systems. *IEEE Transactions on Neural Networks*, *6*(4), 911–917. https://doi.org/10.1109/72.392253

Chen, W., Wang, G., Wu, B., Wang, C., Wang, Y., & Wang, S. (2021). A state-of-the-art survey of transfer learning in structural health monitoring. In Yang, L., Tu, X.W. (ed.) *7th international conference on systems and informatics (ICSAI)* (pp. 1–7). https://doi.org/10.1109/ICSAI53574.2021.9664171

Clough, R., & Penzien, J. (1993). *Dynamics of structures*. McGraw-Hill. https://books.google.co.jp/books?id=HxLakQEACAAJ

Dackermann, U., Li, J., & Samali, B. (2010). Dynamic-based damage identification using neural network ensembles and damage index method. *Advances in Structural Engineering*, *13*(6), 1001–1016. https://doi.org/10.1260/1369-4332.13.6.1001

Entezami, A., Shariatmadar, H., & Michele, C. D. (2022). Nonparametric empirical machine learning for short-term and long-term structural health monitoring. *Structural Health Monitoring*, *21*(6), 2700–2718. https://doi.org/10.1177/14759217211069842

Fernandez-Navamuel, A., Magalhaes, F., Zamora-Sanchez, D., Omella, A. J., Garcia-Sanchez, D., & Pardo, D. (2022). Deep learning enhanced principal component analysis for structural health monitoring. *Structural Health Monitoring*, *21*(4), 1710–1722. https://doi.org/10.1177/14759217211041684

Flah, M., Ragab, M., Lazhari, M., & Nehdi, M. (2022). Localization and classification of structural damage using deep learning single-channel signal-based measurement. *Automation in Construction*, *139*, 104271. https://doi.org/10.1016/j.autcon.2022.104271

Gharehbaghi, V. R., Noroozinejad Farsangi, E., Noori, M., Yang, T., Li, S., Nguyen, A., Málaga-Chuquitaype, C., Gardoni, P., & Mirjalili, S. (2021). A critical review on structural health monitoring: Definitions, methods, and perspectives. *Archives of Computational Methods in Engineering*, *29*(4), 2209–2235. https://doi.org/10.1007/s11831-021-09665-9

Goi, Y., & Kim, C. W. (2017). Damage detection of a truss bridge utilizing a damage indicator from multivariate autoregressive model. *Journal of Civil Structural Health Monitoring*, *7*, 153–162. https://doi.org/10.1007/s13349-017-0222-y

Gomez-Cabrera, A., & Escamilla-Ambrosio, P. J. (2022). Review of machine-learning techniques applied to structural health monitoring systems for building and bridge structures. *Applied Sciences*, *12*(21), 10754. https://doi.org/10.3390/app122110754

Gordan, M., Sabbagh-Yazdi, S.-R., Ismail, Z., Ghaedi, K., Carroll, P., McCrum, D., & Samali, B. (2022). State-of-the-art review on advancements of data mining in structural health monitoring. *Measurement*, *193*, 110939. https://doi.org/10.1016/j.measurement.2022.110939

Hassanpour, A., Moradikia, M., Adeli, H., Khayami, R., & Shamsinejadbabaki, P. (2019). A novel end-to-end deep learning scheme for classifying multi-class motor imagery electroencephalography signals. *Expert Systems*, *36*, e12494. https://doi.org/10.1111/exsy.12494

Hou, R., & Xia, Y. (2021). Review on the new development of vibration-based damage identification for civil engineering structures: 2010–2019. *Journal of Sound and Vibration*, *491*, 115741. https://doi.org/10.1016/j.jsv.2020.115741

Iannelli, P., Angeletti, F., Gasbarri, P., Panella, M., & Rosato, A. (2022). Deep learning-based structural health monitoring for damage detection on a large space antenna. *Acta Astronautica*, *193*, 635–643. https://doi.org/10.1016/j.actaastro.2021.08.003

ISO 8608. (2016). *Mechanical vibration—Road surface profiles—Reporting of measured data* (Standard). International Organization for Standardization.

Kim, C. W., Inoue, S., Sugiura, K., McGetrick, P., & Kawatani, M. (2016). Extracting bridge frequencies from dynamic responses of two passing vehicles. In Zingoni, A. (ed.) *The 6th international conference on structural engineering, mechanics and computations* (pp. 1858–1864). https://doi.org/10.1201/9781315641645-307

Kim, C. W., Kawatani, M., & Kim, K. (2005). Three-dimensional dynamic analysis for bridge–vehicle interaction with roadway roughness. *Computers & Structures*, *83*, 1627–1645. https://doi.org/10.1016/j.compstruc.2004.12.004

Kot, P., Muradov, M., Gkantou, M., Kamaris, G. S., Hashim, K., & Yeboah, D. (2021). Recent advancements in non-destructive testing techniques for structural health monitoring. *Applied Sciences*, *11*(6), 2750. https://doi.org/10.3390/app11062750

Kovachki, N., Li, Z., Liu, B., Azizzadenesheli, K., Bhattacharya, K., Stuart, A., & Anandkumar, A. (2021). *Neural operator: Learning maps between function spaces. CoRR*, *abs/2108.08481*. https://arxiv.org/abs/2108.08481

Li, Z., Kovachki, N., Azizzadenesheli, K., Liu, B., Bhattacharya, K., Stuart, A., & Anandkumar, A. (2020). *Fourier neural operator for parametric partial differential equations*. http://arxiv.org/abs/2010.08895citearxiv:2010.08895

Li, Z., Park, H., & Adeli, H. (2016). New method for modal identification of super high-rise building structures using discretized synchrosqueezed wavelet and Hilbert transforms. *The Structural Design of Tall and Special Buildings*, *26*, e1312. https://doi.org/10.1002/tal.1312

Lin, K., Xu, Y.-L., Lu, X., Guan, Z., & Li, J. (2021). Digital twin-based collapse fragility assessment of a long-span cable-stayed bridge under strong earthquakes. *Automation in Construction*, *123*, 103547. https://doi.org/10.1016/j.autcon.2020.103547

Luo, B., Wang, H., Liu, H., Li, B., & Peng, F. (2019). Early fault detection of machine tools based on deep learning and dynamic identification. *IEEE Transactions on Industrial Electronics*, *66*(1), 509–518. https://doi.org/10.1109/TIE.2018.2807414

Malekloo, A., Ozer, E., AlHamaydeh, M., & Girolami, M. (2021). Machine learning and structural health monitoring overview with emerging technology and high-dimensional data source highlights. *Structural Health Monitoring*, *21*(4), 1906–1955. https://doi.org/10.1177/14759217211036880

Martins, G. B., Papa, J. P., & Adeli, H. (2020). Deep learning techniques for recommender systems based on collaborative filtering. *Expert Systems*, *37*(6), e12647. https://doi.org/10.1111/exsy.12647

McGetrick, P. J., Kim, C.-W., González, A., & Brien, E. J. O. (2015). Experimental validation of a drive-by stiffness identification method for bridge monitoring. *Structural Health Monitoring*, *14*(4), 317–331. https://doi.org/10.1177/1475921715578314

Oh, B. K., Kim, K. J., Kim, Y., Park, H. S., & Adeli, H. (2017). Evolutionary learning based sustainable strain sensing model for structural health monitoring of high-rise buildings. *Applied Soft Computing*, *58*, 576–585. https://doi.org/10.1016/j.asoc.2017.05.029

Perez-Ramirez, C. A., Amezquita-Sanchez, J. P., Valtierra-Rodriguez, M., Adeli, H., Dominguez-Gonzalez, A., & Romero-Troncoso, R. J. (2019). Recurrent neural network model with Bayesian training and mutual information for response prediction of large buildings. *Engineering Structures*, *178*, 603–615. https://www.sciencedirect.com/science/article/pii/S0141029618307235. https://doi.org/10.1016/j.engstruct.2018.10.065

Pezeshki, H., Adeli, H., Pavlou, D., & Siriwardane, S. (2023). State of the art in structural health monitoring of off-shore and marine structures. *Proceedings of the Institution of Civil Engineers—Maritime Engineering*, *176*, 1–40. https://doi.org/10.1680/jmaen.2022.027

Rafiei, M. H., & Adeli, H. (2017a). Neews: A novel earthquake early warning model using neural dynamic classification and neural dynamic optimization. *Soil Dynamics and Earthquake Engineering*, *100*, 417–427. https://doi.org/10.1016/j.soildyn.2017.05.013

Rafiei, M. H., & Adeli, H. (2017b). A novel machine learning-based algorithm to detect damage in high-rise building structures. *The Structural Design of Tall and Special Buildings*, *26*(18), e1400. https://doi.org/10.1002/tal.1400

Rafiei, M. H., Khushefati, W. H., Demirboga, R., & Adeli, H. (2017). Supervised deep restricted Boltzmann machine for estimation of concrete. *Materials*, *114*, 237–244.

Reyes-Carmenaty, G., & Pérez, M. A. (2022). Use of transfer learning for detection of structural alterations. *Procedia Computer Science*, *200*, 1368–1377. https://doi.org/10.1016/j.procs.2022.01.338 [3rd International Conference on Industry 4.0 and Smart Manufacturing]

Rizzo, P., & Enshaeian, A. (2021). Challenges in bridge health monitoring: A review. *Sensors*, *21*(13), 4336. https://doi.org/10.3390/s21134336

Toh, G., & Park, J. (2020). Review of vibration-based structural health monitoring using deep learning. *Applied Sciences*, *10*(5), 1680. https://doi.org/10.3390/app10051680

Wang, J. J., Liu, Y. F., Nie, X., & Mo, Y. L. (2022). Deep convolutional neural networks for semantic segmentation of cracks. *Structural Control and Health Monitoring*, *29*(1), e2850. https://doi.org/10.1002/stc.2850

Yang, Y. B., & Lin, C. W. (2005). Vehicle–bridge interaction dynamics and potential applications. *Journal of Sound and Vibration*, *284*(1-2), 205–226. https://doi.org/10.1016/j.jsv.2004.06.032

Yokoyama, T., Hasegawa, S., Kim, C. W., Saito, T., & Ikeda, D. (2022). Feasibility investigations on bridge damage detection using BWIM focusing on changes in deflection influence line. *Journal of Structural Engineering. A*, *68A*, 329–341. https://doi.org/10.11532/structcivil.68A.329

Yuen, K.-V., & Huang, K. (2018). Identifiability-enhanced Bayesian frequency-domain substructure identification. *Computer-Aided*

Civil and Infrastructure Engineering, *33*(9), 800–812. https://doi.org/10.1111/mice.12377

Yuen, K.-V., Kuok, S.-C., & Dong, L. (2019). Self-calibrating Bayesian real-time system identification. *Computer-Aided Civil and Infrastructure Engineering*, *34*(9), 806–821. https://doi.org/10.1111/mice.12441

Kankanamge, Y., Hu, Y., & Shao, X. (2020). Application of wavelet transform in structural health monitoring. *Earthquake Engineering and Engineering Vibration*, *19*(2), 515–532. https://doi.org/10.1007/s11803-020-0576-8

How to cite this article: Kaewnuratchadasorn, C., Wang, J., & Kim, C. W. (2023). Neural operator for structural simulation and bridge health monitoring. *Computer-Aided Civil and Infrastructure Engineering*, 1–19. https://doi.org/10.1111/mice.13105